Contrib Mineral Petrol (1992) 109:494–510

Contributions to Mineralogy and Petrology

Phase equilibria and oxygen isotopes in the evolution of metapelitic migmatites: a case study from the Pre-Alpine basement of Northern Switzerland

Martin Mazurek

Mineralogisch-petrographisches Institut, Bernoullistrasse 30, CH-4056 Basel, Switzerland

Received November 6, 1989/Accepted May 22, 1991

Abstract. Metapelites that have undergone variable degrees of migmatization were encountered in two deep boreholes in Northern Switzerland. Microtextures and calculated phase diagrams yield three successive stages of metamorphism, consistent with one *P-T* loop: (1) Amphibolite-grade metamorphism (biotite-sillimanite-garnet-oligoclase-quartz-ilmenite), *P–T* conditions are estimated at 4.5–6.5 kbars/550–650 °C. (2) Anatectic migmatization at < 4.5 kbars/> 650 °C. Liquid was generated by incongruent melting reactions. Leucosomes do not represent pure crystallized melt but rather a mixture of melt, cordierite and K-feldspar grown at the expense of biotite and sillimanite. (3) Retrograde hydration, recorded by the growth of large amounts of muscovite at the expense of cordierite and K-feldspar, *P–T* conditions are estimated at < 2.5 kbars/< 600 °C. Oxygen isotope measurements were obtained for whole-rocks and eight mineral species. Isotopic equilibrium among three or even four minerals grown during stage 1 can be demonstrated. Calculated isotopic temperatures are consistent with phase petrology. Migmatization did not re-equilibrate the isotopic composition of the pre-existing quartz grown in stage 1 even over distances as little as 10 cm. High $\delta^{18}O$ in migmatitic quartz is best explained by disequilibrium melting in coexistence with an infiltrating, isotopically heavy fluid. Lack of equilibration of oxygen isotopes between different quartz generations suggests that mineralogical and geochemical changes were rapid relative to diffusion rates. A meteoric-hydrothermal alteration at 300–400 °C, probably genetically linked to the intrusion of Variscan granites, strongly affected the rocks. Quartz did not exchange isotopes with hydrothermal fluids except in segregations where it is recrystallized. The $\delta^{18}O$ values of micas, feldspars and cordierite are often very low and fractionations with quartz very large, which reflects significant hydrothermal effects that were previously detected in the Black Forest by other workers.

Present address: Mineralogisch-petrographisches Institut, Baltzer-Strasse 1, CH-3012 Bern, Switzerland

Introduction

The basement of Northern Switzerland represents the subsurface continuation of the Black Forest Massif of Germany and is covered by Carboniferous to Tertiary (+ / − Quaternary) sediments of greatly varying thickness. It is part of the Pre-Alpine basement of Central Europe, which typically consists of high-grade paragneisses and orthogneisses of Caledonian metamorphic age, which were intruded by Variscan granites. Metapelitic migmatites very similar to those in the Black Forest are known from the Alps (Aar Massif, Abrecht 1980; Rutishauser and Hügi 1978; Schaltegger 1986; Aiguiles Rouges Massif, Von Raumer 1983). To date, the basement of Northern Switzerland has been penetrated by 16 boreholes in the course of exploration for oil, gas, coal, salt, geothermal water and, in recent years, radioactive waste storage. The present study is based on samples from boreholes at Kaisten and Leuggern which were recently drilled by NAGRA (Swiss cooperative for the storage of radioactive waste; see Fig. 1). These sites are the only ones so far to yield predominantly metapelitic gneisses in various stages of migmatization. Each of the boreholes comprises a complete core profile of 9 cm-diameter cores through more than 1,000 meters of the gneiss series (Kaisten, 297–1306 m; Leuggern, 223–1386 m below surface). The nearest surface outcrops of Black Forest basement are only a few kilometers north of the drilling sites (see Fig. 1; Metz 1980; Wimmenauer 1984). NAGRA's boreholes in Northern Switzerland present the first opportunity to examine the basement at a depth where large portions of the rocks underwent less of the weathering and alteration that are pervasive in surface outcrops of the Black Forest (Simon 1989, 1990; Simon and Hoefs 1987; Hoefs and Emmermann 1983).

The aim of this study is to characterize the metapelitic rocks in terms of pressure-temperature evolution and to elucidate the processes and mechanisms that led to migmatite formation. Also, effects of a late hydrothermal overprint will be studied. This paper is concerned with the results of quantitative phase equilibria and oxygen isotope geochemistry.

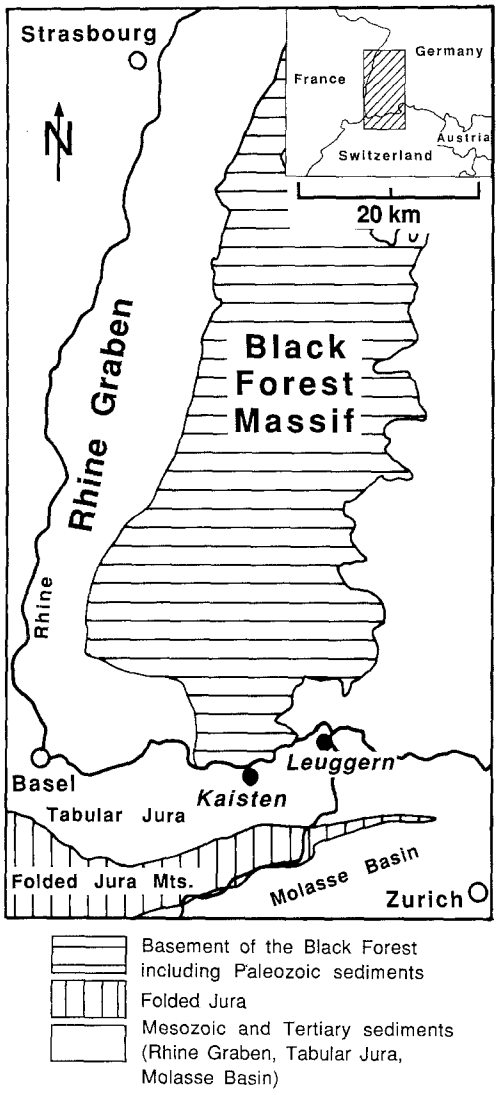

Fig. 1. Geographical setting of the boreholes investigated. The nearest surface outcrops of the Black Forest basement (gneisses and granites) are only a few km to the North

Regional setting

The Black Forest is a classical area of migmatite research (e.g. Mehnert 1953, 1957, 1962, 1963; Busch 1966). In spite of the relatively modest outcrop area and low relief, many new ideas for migmatite genesis originated here. Much attention has been given to Black Forest migmatitic orthogneisses of granitic to tonalitic compositions, but comparatively little petrological work has been done on those of pelitic composition.

The high-grade metapelitic paragneisses are Proterozoic metasediments (Hofmann and Köhler 1973; Wimmenauer 1985), whose burial and metamorphism culminated in regional migmatite formation in the early Paleozoic. The migmatization is dated at 490 + / − 26 Ma (Hofmann and Köhler 1973, Rb/Sr on whole rocks) and at 480 + / − 20 Ma (Steiger et al. 1973, U/Pb on zircon, upper intersection with Concordia) and is attributed to the Caledonian orogeny. Eclogites preserved in basic rocks embedded in the gneisses of the Middle Black Forest (Klein and Wimmenauer 1984) predate migmatite formation, but it is unclear whether they are a direct precursor to the thermal maximum of metamorphism or represent exotic relics of significantly older age. A series of granitic intrusions formed during the Variscan orogeny, of which the oldest are slightly gneissose. The extent of Variscan metamorphism and deformation is as yet unclear. No modification of Caledonian gneiss can be attributed clearly to the Variscan orogeny.

Analytical methods

Phase compositions were determined on an ARL-SEMQ microprobe with four spectrometers and an energy dispersive system, using natural and synthetic silicates and oxides as standards (measuring time, 10 s; voltage, 15 kV; beam current, 20 nA). A ZAF correction was applied and all Fe was assumed to be Fe^{2+}.

Phase diagrams were calculated on an Apple Macintosh SE/30 computer using PTAX, a 1990 upgrade of the FORTRAN code PT-SYSTEM by Perkins et al. (1986) and Brown et al. (1989) and a version of the thermodynamic database of Berman (1988) updated in February 1989. The H_2O fugacities were calculated using the equation of Haar et al. (1984). Model reactions were determined in the system KMASH for the end-member phases andalusite, clinochlore, corundum, cordierite, enstatite, K-feldspar, kyanite, muscovite, phlogopite, pyrope, α-quartz, sillimanite, spinel, and hydrous fluid. Quartz and hydrous fluid were considered as excess phases. In order to correct for non end-member phase chemistries, mineral compositions averaged over several samples (see Table 1) were used for the calculation of activities. Cross-biotite, cordierite from mesosomes and K-feldspar from mesosomes (Tables 1, 2) were the mineral generations used for the calculation of activities. Nonideal, temperature-dependent mixing properties (an option of the program) were taken into account for garnet (Berman 1990), biotite (Indares and Martignole 1985), white mica (Chatterjee and Froese 1975) and alkali feldspar (Fuhrman and Lindsley 1988). Positive deviation from ideality is considerable for pyrope and phlogopite whereas muscovite and K-feldspar show only minor negative deviations. Ideal mixing behaviour was assumed for chlorite (activity model similar to the one used by Graham et al. 1983; tetrahedral mixing neglected) and cordierite. Variable H_2O contents of cordierite as a function of P, T are based on the data of McPhail (1985). All other phases were assumed to be pure.

Oxygen isotope measurements were performed in 16 samples, including 24 whole-rock and 46 mineral analyses. The samples include gneissic rock portions, leucosomes and quartz-rich segregations. Wherever possible mesoscopically different rock portions (i.e. mesosomes—leucosomes—melanosomes) were treated separately. Standard techniques were used for mineral separation (magnetic separation, heavy fluids, handpicking, selective etching with concentrated HF). All the extractable minerals were analysed from each sample. The separation was in part very difficult due to intimate intergrowth of the phases. Plagioclase generally could not be separated, because its specific gravity overlaps with quartz and because of the common occurrence of tiny inclusions of biotite, quartz and accessory phases such as apatite. The purity of the mineral concentrates was controlled systematically by optical inspection and X-ray diffractometry and is estimated to be better than 99%. Measurements of $\delta^{18}O$ were performed by S. Hoernes and coworkers (Bonn, Germany). Oxygen was liberated using a modified fluorine line described by Taylor and Epstein (1962). Powders were disintegrated at 500–700 °C and fluorine pressures of 2–5 bars. Reaction yield was better than 98% in all cases. Double analyses were performed for all samples. Analytical reproducibility is better than + / − 0.1‰ in most cases, and all data refer to standard mean ocean water.

Petrography and phase chemistry of the metapelites

Descriptive terms such as "leucosome", "melanosome" and "mesosome" are used according to the definitions given by Ashworth (1985, pp. 3–4). "Mesosome" rather than the genetic term "paleosome" is used to describe rock portions within migmatites that look like ordinary meta-

morphic rocks. A "mesosome" is not necessarily the non-migmatitic parent rock of the migmatites (see Henkes and Johannes 1981).

Rock types and degrees of migmatization

Rock types in the Kaisten and Leuggern boreholes are mainly of metapelitic composition. Meter-scale intercalations of biotite-plagioclase gneiss, interpreted as metagraywacke according to geochemical discrimination diagrams (Garrels and MacKenzie 1971; De La Roche 1972), are common. Zones of calc-silicate layers and hornblende-bearing gneisses can also be identified but are less common (see Mazurek 1988; Peters et al. 1989a, b for detailed petrographic description). The volume proportion of leucosomes in the metapelitic rocks is estimated at 10%, whereas all other rock types are non-migmatitic.

The degree of migmatization in the metapelites varies strongly on a scale of meters, which is a consequence of either variable H_2O availability during migmatization or different whole-rock compositions within a layered protolith. It is suggested that variable degrees of migmatization are due to variations in H_2O activity; these variations are a consequence of regional deformation (predating migmatization) which caused channelling of the fluid pathways in highly deformed zones.

A certain scatter of whole-rock compositions is present in the rocks (as can be expected in a metasedimentary series). However, there are no statistically significant compositional differences (SiO_2, alkalis, Fe/Mg, $\delta^{18}O$ etc.) of non-migmatitic gneisses (homogeneous on the scale of 5–10 m) and dm-thick mesosomes within the migmatites (Mazurek 1988). In places, zones of homogeneous gneiss are associated with 10–50 m-thick, calcite-bearing calc-silicate layers. These gneisses were not affected by migmatization due to the presence of CO_2 which diluted the hydrous fluid in the vicinity of the calc-silicates. Whole-rock compositions of these gneisses are identical to those of gneisses not associated with calc-silicates, which suggests that these rocks remained non-migmatitic due to lack of H_2O and not due to unsuitable whole-rock compositions. Therefore, it is argued that thicker layers of homogeneous gneiss approximate the protolith of the migmatites.

Macroscopic features and leucosome types

The best-preserved (i.e. least-migmatitic) gneissic rock portions consist of *sillimanite-biotite gneisses* and are garnet bearing in places. The majority of the gneisses, however, contain limited amounts of cordierite and K-feldspar which are associated with the regional migmatization event. The *migmatites* consist of gneissic rock portions (mesosomes) and generally coarse-grained leucosomes which only rarely are surrounded by thin, biotite-rich melanosomes. Mesosomes in the migmatites contain considerable amounts of K-feldspar and cordierite interpreted to have grown at the expense of sillimanite and biotite. The gneissose fabric is destroyed partially by these transformations. The migmatites contain the following leucosome types:

1. Coarse-grained (> 5 mm), cordierite-rich (10–20 vol %) type, most common of all leucosomes (> 98%). This type is the only one considered here.
2. Fine-grained (< 1 mm), tonalitic type with cm-scale cordierite patches
3. Coarse-grained type with an internal zonation (K-feldspar + quartz at the rims, cordierite + quartz in the centres).

Apart from these types, quartz-rich segregations, interpreted as pre-migmatitic subsolidus veins, occur both in the migmatites and in the homogeneous gneisses.

Thickness of type 1 leucosomes ranges from 5 to 30 cm. The leucosomes contain two feldspars, quartz and cordierite. In a few cases, rotated and partly assimilated inclusions of gneiss can be identified (see Fig. 2a). These rafts are a strong argument for the presence of a melt phase, because no ductile deformation postdates migmatite formation. This is also supported by the whole-rock compositions of these leucosomes (Mazurek 1988), which lie close to a granite minimum melt composition. The leucosomes are either subparallel to the pre-migmatitic schistosity and form stromatic migmatites (nomenclature of Mehnert 1968), or they may cross cut the foliation, forming complicated, ragged contacts. No sharp intrusive contacts between leucosomes and paleosomes can be observed. In several samples the leucosomes are subspherical and surrounded by gneiss on all sides, which argues against injection of externally derived melt. All the evidence indicates that this leucosome type crystallized from a melt that was generated in place or within a few dm of its site of crystallization.

Microtextures

Three stages of metamorphic evolution can be distinguished petrographically in the metapelites:

1. *Amphibolite-grade metamorphism and associated deformation* recorded in the homogeneous gneisses, characterized by a strong foliation (defined by biotite and sillimanite). A younger biotite generation cross cuts this foliation in places, but is not abundant. Both biotite generations are pre-migmatitic. Garnet is present in small amounts, often as inclusions in plagioclase. Other phases include: oligoclase, quartz, accessory zircon, apatite, tourmaline and ilmenite. If a few samples, armoured relics of kyanite and staurolite are included within oligoclase. Typical modal compositions according to visual estimates are: Quartz and plagioclase 20–30% each, biotite 25–35%, sillimanite 10–20%.
2. *Migmatite formation* leaves a profound textural imprint in most of the metapelitic rocks (see Fig. 2a, b). Apart from segregation of leucosomes, the main effect of migmatization was the growth of cordierite and K-feldspar even in the still-gneissose rock portions, causing a partial destruction of the pre-existing foliation as defined by biotite and sillimanite. Leucosomes are often very cordierite rich (up to 20%). Because cordierite and K-feldspar commonly include partially resorbed relics of biotite and sillimanite

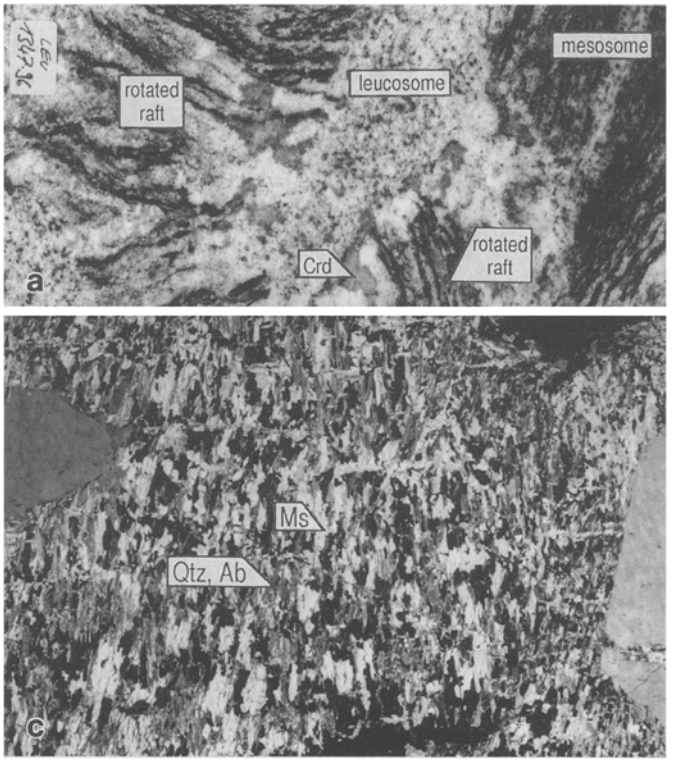

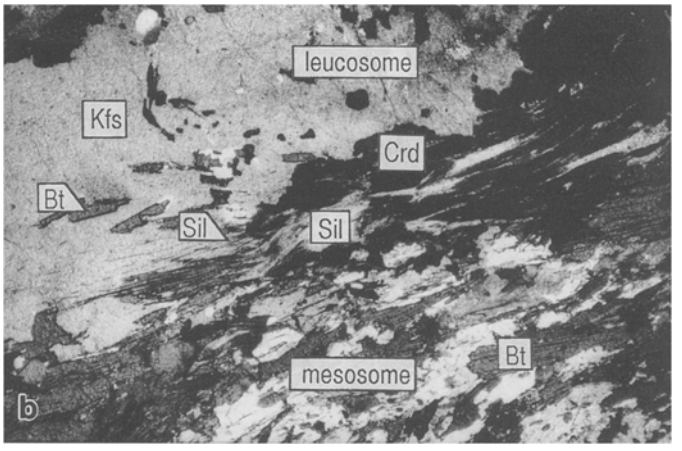

Fig. 2a–c. Photographs of the metapelitic rocks: **a** Coarse-grained, cordierite-rich leucosome including two rotated and partially assimilated rafts of metapelitic gneiss (*left* and *bottom centre*). The foliation of the surrounding mesosome (*right*) runs NE-SW and is cut by the leucosome. Sample LEU 1347.96, height of photograph 9 cm. **b** Microtextures of stage 2: micrograph illustrating the transformation of biotite and fibrolitic sillimanite (both *lower right* and *centre*) to coarse-grained K-feldspar (*upper left*) and cordierite (*black, upper right*). The *upper left half* of the photograph belongs to a coarse-grained, cordierite-rich leucosome, the *lower right half* is a mesosome. Sample LEU 1277.40, height of photograph 4.5 mm, crossed polars. **c** Microtextures of stage 3: retrograde pseudomorph after K-feldspar containing muscovite, albite and quartz. The N-S alignment of crystal intergrowth and W-E trending muscovite trails are relics of the microcline structure. Sample KA1 629.64, sample height 25 mm, crossed polars

(even in the leucosomes), it appears that the cordierite and K-feldspar have grown at the expense of these minerals. There is no evidence for a deformational event associated with migmatite formation.

3. *Retrograde hydration* is locally intense and results in the development of pseudomorphic textures. Approximately 50% of all cordierite present was altered to aggregates of muscovite with some green biotite and quartz. Most of the remaining cordierite was altered to clay minerals during late post-metamorphic hydrothermal events discussed below. More remarkable is the alteration of K-feldspar crystals to conspicuous intergrowths of muscovite, albite, quartz and very rarely andalusite (see Fig. 2c). About half the K-feldspar was transformed in this manner. Both gneissose and leucosomatic rock portions were affected by retrograde reactions, with no apparent preference.

The stabilities of the minerals during the three stages of evolution defined above are represented in Fig. 3. Textures suggest that the three stages, successive in time, represent different stages of a simple P–T path of burial, heating and uplift (i.e. they do not represent separate metamorphic events).

Correlation of textures and phase chemistry

Mean chemical compositions of minerals (average values of all rocks analysed) are presented in Table 1. Chemical comparisons of different textural types of the same mineral were always based on data from the same sample in order to exclude artefacts caused by different whole-rock compositions.

Biotite. There are two prograde biotite generations, one parallel to the foliation and the other cross-cutting it. Both of them are pre-migmatitic because they show the same resorption features, reacting to cordierite and K-feldspar which are related to migmatization. There is a slight but statistically significant decrease of Fe/Mg between biotite aligned in the foliation and cross-biotite from the same sample. It is a striking fact that prograde biotite generations show variable compositions whereas no appreciable zonation in garnet could be identified. A possible explanation would be a slight retrograde Fe/Mg exchange, but it remains unclear why this should be the case in one biotite generation only. The retrograde green-biotite generation, which is optically quite distinct from all prograde biotites, is much more Mg rich than all other biotite types. Its exchange chemistry was probably controlled by (more Mg-rich) cordierite from which it formed.

Garnet, cordierite and K-feldspar. Apart from a slight increase of Mn in the outermost garnet rims, no zonation at all was detected in these phases. The compositions of cordierite and K-feldspar show no significant differences between mesosomes and leucosomes.

Plagioclase. Plagioclase grown during stages 1 and 2 has oligoclase composition (about 20 mol% An component on the average). There is no chemical difference between gneissose rock portions and leucosomes. Chemical

profiles through plagioclase grains often show an unsystematic zigzag pattern with variations in anorthite content of up to 10 mol%. A fine-grained chemically distinct albite generation (> 98 mol% albite) formed during retrograde hydration (stage 3).

Phase relations

The petrogenetic P–T grid

Metamorphic phase equilibria of metapelitic rock compositions in the systems KMASH and KFASH have received considerable attention in recent years (Thompson 1982; Vielzeuf and Boivin 1984; Grant 1985). These authors showed that *P–T* grid topologies are different in KMASH and KFASH, mainly due to the contrasting thermodynamic properties of pyrope and almandine garnet. Recently, Pattison (1989) calculated quantitative phase equilibria both for the pure systems KMASH and KFASH, Powell and Holland (1990) and Spear and Cheney (1990) for KMASH, KFASH and KFMASH, the latter using the Gibbs method.

The present paper presents a grid based on a 1989 update of the Berman (1988) data base for the system KMASH, corrected for measured mineral compositions as listed in Table 1. Therefore, this grid is only applicable to the rocks investigated and also approximative because the averaged phase compositions used as input do not all represent equilibrium relations (e.g. peak-metamorphic versus retrograde assemblages). Analogous calculations in the system KFASH have also been performed and show that the topology is very similar between KMASH and KFASH in the high-temperature part of the grid. The invariant point IP2 lies at 4.2 kbars/650 °C in KFASH, i.e. deviates only slightly from the KMASH grid. However, significant deviations were identified in the low-temperature part of the grid, mainly due to the presence of staurolite in the KFASH database. Thus part of the grid presented here may be metastable with respect to staurolite.

All stable reactions, activity models and activities are listed in Table 2 and the resulting calculated petrogenetic *P–T* grid is drawn in Fig. 4. The experimental granite solidus of Johannes (1985) is added to the calculated equilibria for comparison. The intersections of the solidus with univariant reactions produce invariant points from which further melting reactions emanate, as shown schematically in Fig. 4. Melting reactions are formulated with plagioclase on the reactant side. All reactions observed in the rocks are represented in the calculated phase diagram.

Discussion of relevant subsolidus and melting reactions

Stage 1—amphibolite-grade metamorphism. The gneisses of stage 1 are characterized by the coexistence of biotite, sillimanite, and garnet (but not K-feldspar). These phases

Table 1. Mean chemical compositions (averaged over several samples) of different mineral generations

	Biotite parallel to foliation	Cross-biotite	Biotite included in plagioclase	Biotite relics in leucosomes	Retrograde green biotite	Garnet	Cordierite in mesosomes	Cordierite in leucosomes	K-feldspar in mesosomes	K-feldspar in leucosomes	Plagioclase in mesosomes	Plagioclase in leucosomes	Retrograde albite	Retrograde muscovite	Retrograde chlorite
SiO_2	34.64	34.65	34.67	35.43	34.48	37.57	48.31	48.27	65.43	65.14	63.59	62.57	66.82	46.72	25.47
Al_2O_3	19.07	19.10	19.77	18.61	19.70	21.02	31.92	31.62	18.98	18.93	23.42	24.04	20.41	35.74	20.74
TiO_2	3.58	3.67	3.21	4.10	0.87	0.01	0.03	0.02	0.03	0.04	0.01	0.00	0.00	0.13	0.06
FeO	21.85	22.15	21.52	21.63	20.16	34.17	10.76	10.60	0.02	0.01	0.03	0.03	0.03	1.25	25.64
MnO	0.17	0.21	0.17	0.14	0.31	1.23	0.38	0.49	0.02	0.02	0.00	0.00	0.00	0.00	0.52
MgO	5.69	5.39	5.78	5.85	8.03	2.07	5.55	5.63	0.00	0.00	0.02	0.00	0.00	0.45	12.24
CaO	0.04	0.02	0.07	0.00	0.00	3.50	0.00	0.00	0.02	0.00	4.31	4.92	1.35	0.00	0.00
Na_2O	0.24	0.21	0.10	0.22	0.19	0.00	0.32	0.27	1.69	1.69	8.77	8.89	10.70	0.53	0.00
K_2O	9.59	9.59	9.76	9.66	8.70	0.01	0.00	0.00	13.93	13.93	0.35	0.28	0.10	8.87	0.01
BaO	0.10	0.15	0.00	0.10	0.09	0.03	0.02	0.00	0.44	0.43	0.00	0.00	0.04	0.31	0.05
F	0.30	0.29	0.28	0.14	0.18	0.01	0.00	0.01	0.00	0.10	0.04	0.01	0.00	0.00	0.00
Sum	95.27	95.43	95.33	95.88	92.71	99.62	97.29	96.91	100.56	100.29	100.54	100.74	99.45	94.00	84.73
Si	2.689	2.689	2.681	2.720	2.710	3.041	5.085	5.099	2.987	2.986	2.795	2.754	2.943	3.118	2.789
Al^{IV}	1.311	1.311	1.319	1.280	1.290		0.915	0.901	1.021	1.023	1.213	1.247	1.060	0.882	1.211
Al^{VI}	0.434	0.436	0.483	0.404	0.535	2.006	3.045	3.036						1.929	1.466
Ti	0.209	0.214	0.187	0.237	0.051	0.001	0.002	0.002	0.001	0.001	0.000	0.000	0.000	0.007	0.005
Fe^{++}	1.418	1.438	1.391	1.389	1.325	2.313	0.947	0.936	0.001	0.000	0.000	0.001	0.001	0.001	2.348
Mn	0.011	0.014	0.011	0.009	0.021	0.084	0.034	0.044	0.001	0.000	0.000	0.000	0.000	0.000	0.048
Mg	0.658	0.624	0.666	0.669	0.941	0.250	0.871	0.886	0.000	0.000	0.001	0.000	0.000	0.000	1.998
Ca	0.003	0.002	0.006	0.000	0.000	0.304	0.000	0.000	0.001	0.000	0.203	0.232	0.064	0.000	0.000
Na	0.036	0.032	0.015	0.033	0.029	0.000	0.065	0.055	0.150	0.150	0.747	0.759	0.914	0.069	0.000
K	0.950	0.949	0.963	0.946	0.872	0.001	0.000	0.000	0.811	0.814	0.020	0.016	0.006	0.755	0.001
Ba	0.003	0.005	0.000	0.003	0.003	0.001	0.001	0.000	0.008	0.008	0.000	0.000	0.001	0.008	0.002
F	0.074	0.071	0.068	0.034	0.045	0.003	0.000	0.003	0.000	0.014	0.006	0.001	0.000	0.000	0.000

Formulae are recalculated on the basis of 11 oxygens for biotite and muscovite, 8 cations for garnet, 18 oxygens for cordierite, 8 oxygens for feldspars, and 14 oxygens for chlorite

Table 2. List of end-member phase compositions, abbreviations (following the scheme of Kretz 1983), activity models, ideal activities and reactions represented in Fig. 4. *P*, *T* dependent nonideal activities used for garnet, biotite, muscovite and K-feldspar slightly deviate from the ideal values

Abbreviation	Phase	End-member composition	Activity model	Ideal activity
Ab	Albite	$NaAlSi_3O_8$	–	
Als	Alumosilicates (And, Ky, Sil)	Al_2SiO_5	Pure phase	1
And	Andalusite	Al_2SiO_5	Pure phase	1
Bt	Biotite (phlogopite)	$KMg_3AlSi_3O_{10}(OH)_2$	$X_K^{XII*}(X_{Mg}^{VI})^3$	0.00854
Chl	Chlorite (clinochlore)	$Mg_5Al_2Si_3O_{10}(OH)_8$	$6.75(X_{Mg}^{Brc})^{2*}\ (X_{Al}^{Brc})^*\ (X_{Mg}^{Tlc})^3$	0.0479
Crd	Cordierite	$Mg_2Al_4Si_5O_{18}$	$(X_{Mg}^{VI})^2$	0.190
Grt	Garnet (pyrope)	$Mg_3Al_2Si_3O_{12}$	$(X_{Mg}^{VIII})^3$	0.000579
Kfs	K-feldspar	$KAlSi_3O_8$	X_K^{IX}	0.811
L	Silicate melt			
Ky	Kyanite	Al_2SiO_5	Pure phase	1
Ms	Muscovite	$KAl_3Si_3O_{10}(OH)_2$	$X_K^{XII*}(X_{Al}^{VI})^2$	0.702
Qtz	Quartz	SiO_2	Pure phase	1
Sil	Sillimanite	Al_2SiO_5	Pure phase	1

Subsolidus reactions

(1) $Ms + Qtz = Als + Kfs + H_2O$
(2) $And = Ky$
(3) $Ky = Sil$
(4) $And = Sil$
(5) $8Als + 2\,Chl + 11\,Qtz = 5\,Crd + 8H_2O$
(6) $3\,Crd + 2\,Ms = 8\,Als + 2\,Bt + 7\,Qtz$
(7) $6\,Als + 2\,Bt + 9\,Qtz = 3\,Crd + 2\,Kfs + 2\,H_2O$
(8) $3\,Chl + 5\,Ms = 8\,Als + 5\,Bt + Qtz + 12\,H_2O$
(9) $2\,Bt + 6\,Ms + 15\,Qtz = 3\,Crd + 8\,Kfs + 8\,H_2O$
(10) $Chl + Ms + 2\,Qtz = Bt + Crd + 4\,H_2O$
(11) $2\,Als + 3\,Chl + 4\,Qtz = 5\,Grt + 12\,H_2O$
(12) $2\,Chl + Crd + Qtz = 4\,Grt + 8\,H_2O$
(13) $3\,Crd = 4\,Als + 2\,Grt + 5\,Qtz$

Melting reactions (including albite, stoichiometric coefficients omitted)

(14) $Ab + Kfs + Qtz + H_2O = L$
(15) $Ab + Bt + Kfs + Ms + Qtz + H_2O = L$
(16) $Ab + Als + Bt + Kfs + Qtz + H_2O = L$
(17) $Ab + Crd + Kfs + Qtz + H_2O = L$
(18) $Ab + Bt + Ms + Qtz + H_2O = L + Als$
(19) $Ab + Bt + Ms + Qtz = L + Als + Kfs$
(20) $Ab + Als + Bt + Qtz + H_2O = L + Crd$
(21) $Ab + Als + Bt + Qtz = L + Crd + Kfs$

are stable in a well-confined area at 4.5–6.5 kbars/550–650 °C. Kyanite relics identified in thin section belong to the very early evolution of the gneisses, which possibly took place at even higher pressures.

Stage 2—migmatite formation. Migmatization is characterized by the simultaneous appearance of cordierite, K-feldspar and melt, and consumption of biotite and sillimanite. Relict biotite and minor sillimanite are present as inclusions in cordierite and K-feldspar in leucosomes. This suggests that cordierite and, to some extent, K-feldspar, did not crystallize from the melt, but coexisted with it as a solid phase.

Theoretical and experimental work suggests that melting of metapelitic rocks is considerably more complicated than in the haplogranitic system (e.g. Vielzeuf and Holloway 1988; Puziewicz and Johannes 1988; Patiño Douce and Johnston 1991). Every intersection of an univariant subsolidus equilibrium with the solidus results in an invariant point from which incongruent melting reactions emanate (Thompson 1982). The two invariant points that may be relevant for the present study are IP 4 and IP 5 represented in the grid of Fig. 4. In addition, the presence of plagioclase and a limited solubility of cordierite in the melt (Grant 1985) are assumed in the inset of Fig. 4. Reactions associated with IP 5 only affect muscovite-bearing parageneses and are not considered here (all muscovite is retrograde). Because the pre-migmatitic protolith is K-feldspar-free, the first important melting reaction is

$$\text{plagioclase} + \text{sillimanite} + \text{biotite} + \text{quartz} + H_2O = \text{melt} + \text{cordierite}. \quad (20)$$

This "water-saturated" melting reaction produces cordierite in coexistence with melt, which could explain the observed abundance of cordierite in leucosomes (up to 20 vol%). Hoffer (1978) was able to reproduce this reaction experimentally using natural reactants. This reaction needs water to proceed; arguments for external fluid influx during migmatization will be developed in the section on oxygen isotopes. An alternative to a water-saturated mechanism is the reaction

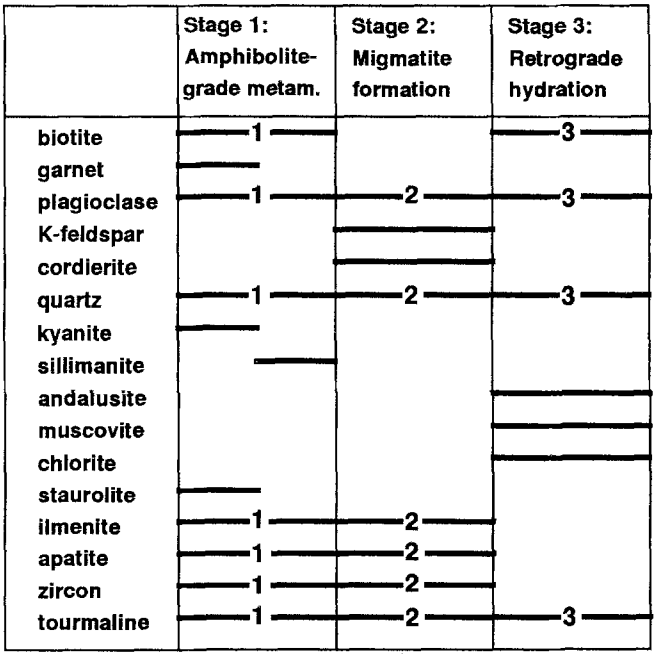

Fig. 3. Mineral growth as a function of the metamorphic evolution, deduced from microtextures. Minerals formed in more than one generation are numbered according to the respective stage of growth. Older generations are often preserved as relics

plagioclase + sillimanite + biotite + quartz = melt + cordierite + K-feldspar, (21)

which is a water-free "dehydration-melting" reaction according to Thompson (1982). The H_2O necessary for melting with reaction (21) is provided solely by hydrous solid reactants and thus this reaction can generate large amounts of melt. It is not entirely clear from petrographic evidence whether H_2O-saturated melting (reaction 20) or dehydration melting (reaction 21) occurred. Mutually parallel biotite and sillimanite inclusions in K-feldspar crystals from leucosomes argue for the dehydration-melting reaction (21) because all K-feldspar generated by reaction (20) crystallized from a melt and thus should not have oriented inclusions. However, isotopic data discussed below indicate some external H_2O influx during migmatization, and this would favour a H_2O-saturated melting reaction such as (20). Therefore it is suggested that both melting mechanisms contributed to migmatite formation, although it remains unclear whether water-saturated melting occurred before or after dehydration melting.

Migmatization (stage 2, Fig. 4) cannot be very well constrained in terms of pressure and temperature. The stability of cordierite with respect to garnet points to pressures below 4.5 kbars (reaction 13, see Table 2), and temperature must have been above the granite solidus, i.e. higher than 650–670 °C. Thus, from metamorphic stage 1 to migmatization, temperature increase was accompanied by pressure release. The geothermal gradient at stage 2 was 40K/km or higher. Le Breton and Thompson (1988) experimentally determined the dehydration-melting reaction

plagioclase + sillimanite + biotite + quartz = melt + garnet + K-feldspar, (22)

which is metastable with respect to the cordierite-producing reaction (21) at low pressures. Taking (22) as an approximation of the upper stability of plagioclase + sillimanite + biotite + quartz under fluid-absent conditions, the temperature of migmatite formation during stage 2 must have exceeded 740–750 °C if dehydration melting was operative.

Stage 3—retrograde hydration. The retrograde hydration was induced by a major H_2O infiltration, which led to the alteration of the migmatitic assemblage cordierite + K-feldspar to muscovite, albite and minor quartz and biotite following a reaction such as

biotite + muscovite + quartz = cordierite + K-feldspar + H_2O. (9)

Albite present in pseudomorphs after K-feldspar represents the albite component of the high-temperature alkali feldspar. Coexistence of andalusite and muscovite indicates upper limits for pressure and temperature of less than 600 °C and less than 2.5 kbars.

Degree of chemical equilibration

As mentioned above, texturally distinct biotite generations show systematic variations in Fe/Mg ratios over distances of only a few mm. These variations cannot be explained by retrograde effects, because in that case all biotite present and not only a single generation should be affected. If selective alteration is ruled out, the preservation of different Fe/Mg ratios in prograde biotite types indicates that regional migmatization was a fast process with respect to diffusion rates of Fe and Mg in biotite. This must also be true for other coexisting minerals, because sheet silicates are among the most reactive phases in metamorphic rocks (Loomis 1983). Plagioclase compositions confirm this conclusion: at equilibrium, the plagioclase component in anatectic melts should be significantly richer in albite than the solid residue (experimentally shown by Yoder et al. 1957; Johannes 1978). This is not the case in the rocks studied here nor in many other natural examples (Mehnert 1968; Ashworth 1976). Ashworth (1985) discussed several ways to explain this inconsistency:

1. *Re-equilibration during crystallization of the melt* is unlikely in the present case because chemical profiles through plagioclase grains often show unsystematic zig-zag patterns both in residues and leucosomes. Thus not even single grains attained chemical equilibrium.
2. *Re-equilibration during retrograde overprint* is unlikely for the same reason. In addition, a chemically distinct albite generation grew during retrograde hydration.
3. *Unstable (i.e. congruent) melting* of plagioclase (Johannes 1983, 1985) is the most likely explanation. Johannes (1983) extrapolated his experiments to geological timescales and found that diffusion rates in plagioclase are extremely slow even at magmatic temperatures, precluding the evolution of a melt richer in albite component than the coexisting solid plagioclase.

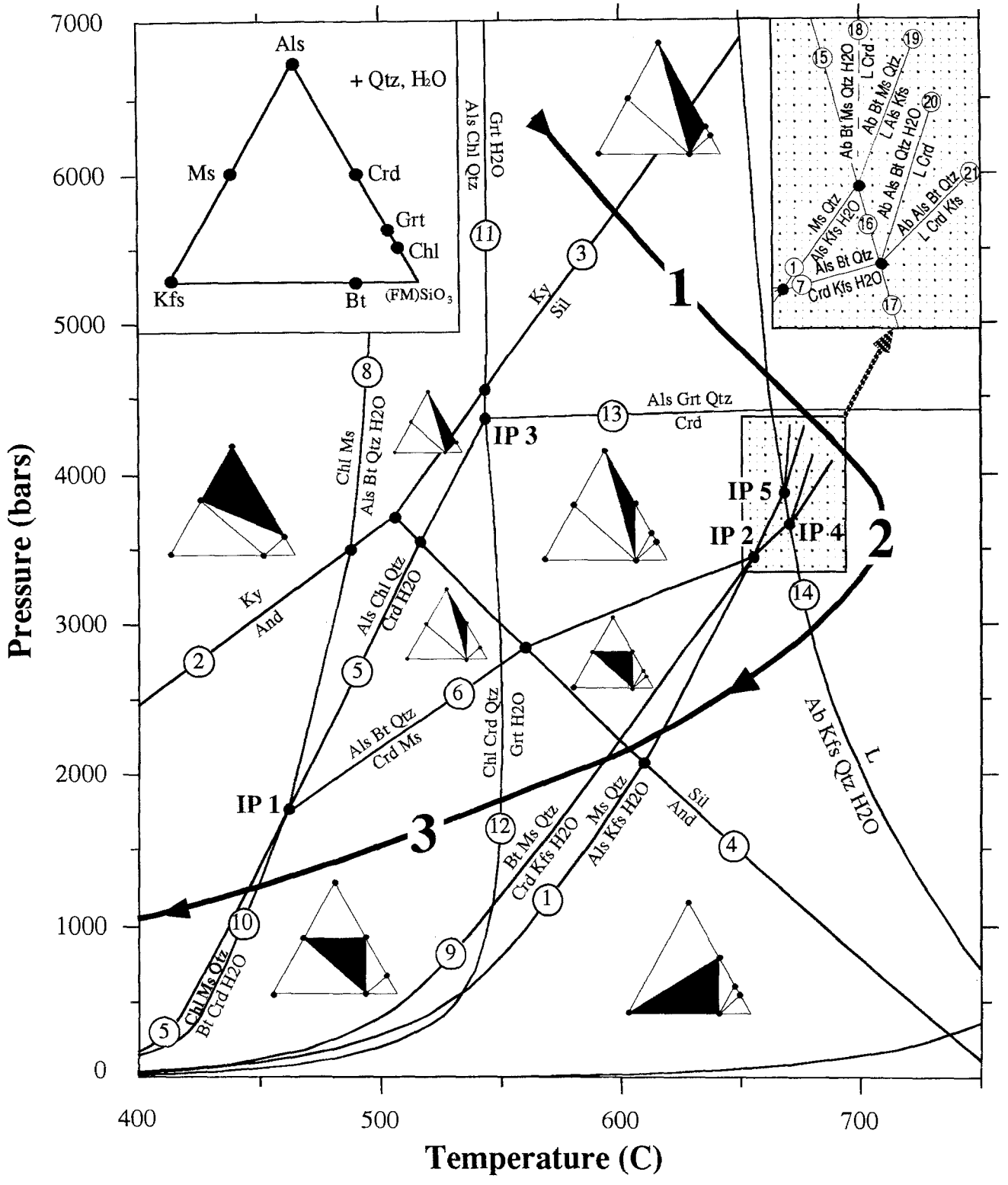

Fig. 4. Calculated phase diagram for metapelites in the system KMASH coexisting with a pure H_2O fluid, corrected for solid solutions and projected from H_2O and quartz. Sodic plagioclase is the only Na- and Ca-bearing solid phase and occurs over the whole *P-T* range. The experimental granite solidus in the system KNASH (Johannes 1985) and some other melting reactions (all including sodic plagioclase) are entered schematically in the inset, where melt is assumed to have a limited solubility for cordierite. *Black areas* in the chemographic projections represent parageneses observed in the rocks. The metamorphic path of the rocks in *P-T* space is given as a *thick solid line*, the three stages of evolution are represented by numbers. *IP* = invariant point

Oxygen isotope geochemistry

The $\delta^{18}O$ values of 24 whole-rocks and 46 minerals were analysed. All results are listed in Table 3, including temperatures calculated from ^{18}O fractionations.

Method of temperature calculation

Experimental calibrations of mineral-water fractionations of oxygen isotopes are not available for some of the minerals analysed (e.g. sillimanite, cordierite). Published data are in part inconsistent and contradictory due to different experimental techniques. A number of calibrations based on empirical and/or thermodynamic data have been developed in recent years. Garlick (1966) found an empirical relation between the Si and Al content of silicate minerals and the relative ^{18}O enrichment. He developed a first expression of ^{18}O fractionation as a function of chemical composition. Schütze (1980) extended this approach by including thermodynamic data (vibrational frequencies) and crystal chemical and structural parameters such as composition, ionic radii and charges, coordination etc. in the model. Oxygen fractionations were derived from thermodynamic data by Bottinga and Javoy (1973, 1975) and Kieffer (1982), which led to internally consistent datasets for a limited number of phases. Unfortunately the latest theoretical approach by Patel et al. (1989) does not include quartz. Also data using the carbonate-exchange technique (Clayton et al. 1989; Chiba et al. 1989) are available so far for a very limited set of minerals.

For the purposes of the present paper the method of Richter and Hoernes (1988) is most suitable; all isotopic temperatures presented below are based upon this approach. The technique is an improved version of Schütze's (1980) increment method, and allows the calculation of internally consistent equilibrium fractionations among any silicate phases and water. For comparison, temperatures were also calculated according to the Bottinga and Javoy (1973, 1975) calibrations where possible. In general, there is a good agreement of the two data sets. The average deviations of the Bottinga and Javoy (1973, 1975) calibrations are + 24 K (quartz-biotite), + 25 K (quartz-alkali feldspar) and + 4 K(quartz-garnet). However, there is a serious discrepancy for muscovite, as quartz-muscovite temperatures show an average deviation of -71 K. Thus using the Bottinga and Javoy (1973, 1975) calibrations leads to lower temperature estimates for phase 3 (retrograde hydration).

$\delta^{18}O$ *of whole-rocks*

Whole-rock data are graphically represented in Fig. 5. They can be divided into five groups, excluding 3 samples (LEU 1010.71, LEU 1011.12, LEU 1363.18) that have extremely low $\delta^{18}O$ values which result from hydrothermal alteration:

1. Homogeneous gneisses with no observable migmatitic overprint within the nearest few meters. According to petrographic evidence, these rocks are interpreted as the parent rocks of the migmatites. Their $\delta^{18}O$ values are in the narrow range of 10.65–10.9‰[1].
2. Mesosomes from migmatite samples show a wider range in $\delta^{18}O$ (10.2–11.05 ‰), overlapping with the samples of group 1.
3. Melanosomes have consistently lower $\delta^{18}O$ values than mesosomes (9.7–9.95 ‰).
4. Leucosomes always have higher $\delta^{18}O$ values than mesosomes (10.65–12.15 ‰).
5. A quartz-rich, pre-migmatitic segregation (with minor K-feldspar) has a $\delta^{18}O$ value of 12.55 ‰.

Discussion. The isotopic compositions of homogeneous gneisses and mesosomes (groups 1 and 2) are typical for high-grade metapelitic gneisses (Hoefs 1987). Leucosomes and segregations are consistently heavier, whereas melanosomes are lighter than mesosomes. This is explained by the relative enrichment of isotopically heavy minerals such as quartz and feldspars in leucosomes, whereas melanosomes are rich in isotopically light biotite. Whole-rock isotopic data are consistent with the hypothesis that the migmatites formed in a closed system, because the mass balance relation

$$\delta^{18}O_{melanosome} < \delta^{18}O_{mesosome} < \delta^{18}O_{leucosome}$$

is not violated.

$\delta^{18}O$ *of quartz*

The $\delta^{18}O$ values of 17 quartz separates are shown in Fig. 6. The results can be divided into the following groups according to petrographic criteria:

1. Quartz from homogeneous gneisses, mesosomes and melanosomes of migmatites, crystallized during amphibolite-grade metamorphism (stage 1). Values of $\delta^{18}O$ lie between 10.5 and 12.5 ‰.
2. Quartz from leucosomes (crystallized from a melt, stage 2) ranges from $\delta^{18}O$ values of 11.4 to 12.95 ‰, which is slightly higher than quartz from group 1.
3. Quartz from segregations that are interpreted as pre-migmatitic exhibits a wide scatter of $\delta^{18}O$ between 7.45 and 12.5 ‰.

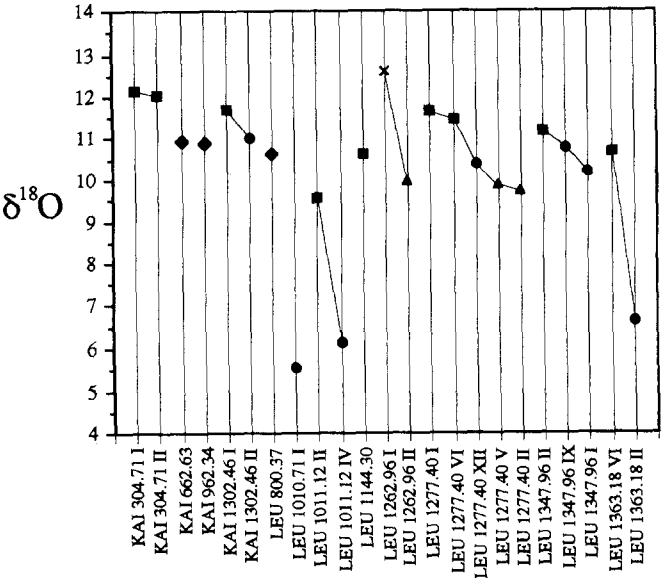

Fig. 5. Measured $\delta^{18}O$ values of whole-rocks. ◆ homogeneous non-migmatitic gneiss, ● mesosome, ▲ melanosome, ■ leucosome, × qtz-rich segregation

[1]All $\delta^{18}O$ values and fractionations reported are rounded to ± 0.05‰.

Table 3. List of all measured $\delta^{18}O$ data of whole-rocks (WR) and minerals

Sample no.	Description	Phase[a]	$\delta^{18}O$ in ‰	Mineral[a] pair	Fractionation	Equil.[b] temp.	Diseq.[b] temp.	Error[c]	Remarks	Temp.[d] B&J
KAI 304.74 I	Tonalitic leucosome type	WR	12.14							
KAI 304.74 II	Leucosome with some gneissic material	WR	12.05							
KAI 547.60	Crd-rich leucosome type	Ms	10.38	Qtz 2-Ms	2.57		647	− 22/ + 23		560
		Qtz 2	12.95							
KAI 662.63	Homogeneous gneiss	WR	10.92							
KAI 889.10	Crd-rich leucosome type	Ms	9.13	Qtz 2-Ms	2.65		636	− 21/ + 22	Plagioclase calculated as	550
		Qtz 2	11.78	Qtz 2-Pl 3	Revers.					
		Pl 3	12.06	Pl 3-Ms	2.93	417		− 16/ + 17	pure albite	317
KAI 962.34	Grt-bearing, homogeneous gneiss	WR	10.86	Qtz 1-Bt	4.69		536	− 11/ + 12	Biotite weakly	562
		Bt	7.45	Qtz 1-Grt	3.47	636		− 16/ + 17	hydrothermally	638
		Grt	8.67	Qtz 1-Sil	1.99	559		− 26/ + 29	altered	
		Qtz 1	12.14	Sil-Bt	2.70		518	− 19/ + 20		
		Sil	10.15							
KAI 1302.46 I	Crd-rich leucosome type	WR	11.70	Qtz 2-Ms	3.0		588	− 18/ + 19	Plagioclase	509
		Ms	9.63	Qtz 2-Pl 3	0.82		741	− 66/ + 82	calculated as	814
		Qtz 2	12.63	Pl 3-Ms	2.18	516		− 23/ + 25	pure albite	392
		Pl 3	11.81							
KAI 1302.46 II	Mesosome	WR	11.04							
		Qtz 1	12.46							
LEU 800.37	Homogeneous gneiss	WR	10.65							
LEU 963.65	Qtz segregation with minor Kfs	Kfs	6.05	Qtz 4a-Kfs	3.37		263	− 11/ + 12	All phases	263
		Ms	2.86	Qtz 4b-Kfs	1.42		532	− 35/ + 41	hydrothermally	553
		Qtz 4a	9.42	Qtz-4a-Ms	6.56		329	− 7/ + 7	altered	281
		Qtz 4b	7.47	Qtz-4b-Ms	4.61		438	− 10/ + 11		377
				Kfs-Ms	3.19		390	− 14/ + 15		296
LEU 992.87	Qtz segregation	Qtz 4	8.48							
LEU 1010.71 I	Mesosome	WR	5.54	Qtz 1-Bt	9.99		296	− 4/ + 4	Biotite	317
		Bt	0.50	Qtz 1-Grt	3.17	671		− 18/ + 19	hydrothermally	681
		Grt	7.32	Qtz 1-Sil	1.41	690		− 39/ + 41	altered	
		Qtz 1	10.49	Sil-Grt	1.76	655		− 31/ + 35		
		Sil	9.08	Sil-Bt	8.58		183	− 4/ + 4		
LEU 1010.71 II	Crd-rich leucosome type	Ms	7.00	Qtz 2-Ms	4.38		455	− 11/ + 12		392
		Qtz 2	11.38							
LEU 1011.12 II	Leucosome with Sil relics	WR	9.57	Qtz 2-Sil	2.23		518	− 23/ + 25	Sillimanite weakly hydrothermally altered	
		Qtz 2	11.50							
		Sil	9.27							
LEU 1011.12 IV	Mesosome	WR	6.16	Qtz 1-Bt	9.66		305	− 4/ + 4	Biotite	327
		Bt	1.42	Qtz 1-Grt	3.58	624		− 16/ + 16	hydrothermally altered	624
		Grt	7.50							
		Qtz 1	11.08							
LEU 1144.30	Tonalitic leucosome type	WR	10.64							
LEU 1262.96 I	Qtz-rich segregation	WR	12.56	Qtz 4-Kfs	1.34	553		− 38/ + 44		578
		Kfs	11.18							
		Qtz 4	12.52							
LEU 1262.96 II	Melanosome	WR	9.93	Qtz 1-Bt	3.69	625		− 15/ + 16	Plagioclase	654
		Bt	8.73	Qtz 1-Kfs	1.01	659		− 53/ + 63	calculated for	707
		Kfs	11.41	Qtz 1-Pl 1	0.83	775		− 66/ + 81	$X(An) = 0.1$	864
		Pl 1	11.59	Qtz 1-Sil	1.84		588	− 29/ + 32		
		Qtz 1	12.42	Kfs-Bt	2.68	611		− 20/ + 22	Sillimanite	637
		Sil	10.58	Kfs-Sil	0.83		486	− 56/ + 71	weakly	
				Pl 1-Bt	2.86	570		− 19/ + 20	hydrothermally	596
				Pl 1-Sil	1.01		351	− 40/ + 49	altered	
				Sil-Bt	1.85		658	− 30/ + 33		
LEU 1277.40 I	Crd-rich leucosome type	WR	11.66	Qtz 2-Crd	2.96		478	− 17/ + 18	Cordierite, K-feldspar hydrothermally altered	
		Crd	9.19	Qtz 2-Kfs	1.16	606		− 45/ + 53		641
		Kfs	10.99	Kfs-Crd	1.80		373	− 24/ + 27		
		Qtz 2	12.15							
LEU 1277.40 II	Melanosome	WR	9.70							
		Bt	7.88							

Table 3. (continued)

Sample no.	Description	Phase[a]	$\delta^{18}O$ in ‰	Mineral[a] pair	Fractionation	Equil.[b] temp.	Diseq.[b] temp.	Error[c]	Remarks	Temp.[d] B&J
LEU 1277.40 V	Melanosome (more leucocratic than II)	WR	9.86							
LEU 1277.40 VI + VII	Crd-rich leucosome type	WR	11.45							
LEU 1277.40 XII	Mesosome	WR	10.40							
LEU 1347.96 I	Mesosome	WR	10.20							
LEU 1347.96 II	Crd-rich leucosome type	WR	11.17							
LEU 1347.96 III + IV	Gneissose raft in leucosome	WR	11.19							
LEU 1347.96 IX + X	Mesosome	WR	10.76							
LEU 1363.18 II	Mesosome	WR	6.65	Qtz-1-Bt	10.75		276	− 4/ + 4	Biotite, K-feldspar hydrothermally altered	297
		Bt	1.75	Qtz 1-Kfs	5.21		159	− 6/ + 6		159
		Kfs	7.29	Kfs-Bt	5.54		363	− 8/ + 8		392
		Qtz 1	12.49							
LEU 1363.18 VI	Crd-rich leucosome type	WR	10.70	Qtz 2-Kfs	3.61		246	− 10/ + 11	Cordierite, K-feldspar hydrothermally altered	245
		Crd	7.35	Qtz 2-Crd	5.42		291	− 7/ + 8		
		Kfs	9.16	Kfs-Crd	1.81		371	− 24/ + 27		
		Qtz 2	12.77							

[a] A number beside the phase name represents the different generations (i.e. stage of metamorphic evolution as defined in Fig. 3); *Qtz 4*, quartz from pre-migmatitic segregations

[b] Temperatures are calculated using the method of Richter and Hoernes (1988) and are separated into columns of equilibrium and disequilibrium temperatures

[c] Error in temperature estimation is calculated by addition/subtraction of 0.15‰ to the fractionation

[d] Temperatures calculated according to Bottinga and Javoy (1973, 1975) for comparison

a. Pre-migmatitic quartz segregations. In one sample (LEU 1262.96) the difference in $\delta^{18}O$ to quartz in the adjacent gneissose rock is 0.1‰ and thus within analytical error. This is consistent with the textural interpretation, attributing these segregations to the amphibolite-grade metamorphism of stage. 1. Two other samples (LEU 963.65, LEU 992.87), however, show extremely low $\delta^{18}O$ values. The isotopic variation of two quartz analyses within the single segregation of sample LEU 963.65 is 2‰. Muscovite and K-feldspar in this sample also show exceedingly low $\delta^{18}O$. These low and scattered $\delta^{18}O$ values are due to late exchange with hydrothermal waters and will be discussed in more detail below.

b. Quartz from gneisses/mesosomes (stage 1) and leucosomes (stage 2). The mean $\delta^{18}O$ value of quartz from leucosomes (crystallized from a melt, stage 2) is 12.15 + / − 0.63 ‰, which is slightly higher than quartz of group 1. In four samples, a direct comparison of quartz in mesosome and adjacent leucosome could be performed, and in all cases, quartz from leucosomes has consistently higher $\delta^{18}O$ values than in the mesosomes only 10–20 cm away. The difference averages 0.45 ‰ and exceeds the analytical error, although, due to the limited number of samples examined, it is difficult to assess the full significance of this result. Nevertheless, the difference should be accounted for and the following mechanisms may explain the isotopic contrast between quartz in leucosomes and gneissose rock portions:

1. *Selective post-migmatitic alteration.* It is conceivable that systematic variations in permeability or other physical properties existed between gneissose rock portions and leucosomes during retrograde hydration and hydrothermal alteration, and this may have led to a very selective post-migmatitic overprint. However, the well-preserved isotopic equilibria of stage 1 in some gneissose rock portions (e.g. LEU 1010.71 I) indicate that the latter are unaffected by any late alteration. Evidence for hydrothermal alteration of quartz was observed only in two coarse-grained segregations, where the effect was an appreciable *lowering* of $\delta^{18}O$ and not the increase necessary to explain isotopically heavy quartz in leucosomes. Therefore, it is suggested that quartz remained unaffected by hydrothermal alteration (with the exception of some segregations discussed in "Isotopic effects of hydrothermal alteration") and another explanation must be found for isotopically heavy quartz in leucosomes. Furthermore, there is no petrographic evidence for a selective overprint of certain rock types.

2. *^{18}O fractionation between melt and solids* has been reviewed by Taylor and Sheppard (1986). Using natural observations such as ^{18}O fractionation between phenocrysts and groundmass in volcanic rocks and $\delta^{18}O$ evolution of magmatic suites (differentiation by fractional crystallization from basaltic magmas), they concluded that there is virtually no fractionation between minerals and liquids of identical composition. Also, Garlick (1966) demonstrated that ^{18}O fractionation is governed by com-

position (mainly Si and Al contents) whereas the physical state (molten or solid) is negligible. Therefore, ^{18}O fractionation between melt and solids cannot explain higher $\delta^{18}O$ in leucosomes.

3. *Disequlibrium melting.* This mechanism is considered most suitable to explain high $\delta^{18}O$ of quartz in leucosomes. It implies infiltration of an externally derived, high $\delta^{18}O$ fluid during migmatization. This fluid would cause water-saturated melting (such as reaction 20 in Table 2) and thus be incorporated in the molten leucosomes.

Migmatite formation took place under conditions of regional uplift and an elevated geothermal gradient, as deduced from phase equilibria, and this may have favoured the mobility of the fluid phase and infiltration into the migmatites. The origin of the infiltrated fluid remains unclear, its $\delta^{18}O$ value was around 11–11.5 ‰ (calculated after Richter and Hoernes 1988 at 670 °C), which is heavier by about 2–3 ‰ than "magmatic water" as defined by Sheppard (1986) but falls into the range of water in equilibrium with S-type granites (Sheppard *et al.* 1969; Sheppard 1977, 1986; O'Neil and Chappell 1977). However, there is no field evidence for the crystallization of S-type granites at the time of migmatite formation. Migmatites are a regional phenomenon in the Black Forest basement and are not spatially coupled to granites. The infiltrated water was probably of metamorphic origin, and cannot be further characterized at present.

$\delta^{18}O$ of other minerals

In addition to quartz, $\delta^{18}O$ values were determined for garnet, sillimanite, plagioclase/albite, K-feldspar, cordierite, muscovite, and biotite (Table 3). One single reversal could be identified, all other samples show the order of relative $\delta^{18}O$ enrichment required for equilibrium. However, temperature calculation reveals many isotopic disequilibria, best explained by two effects:

1. Disequilibria among minerals not belonging to the same stage of metamorphic evolution.
2. Hydrothermal alteration preferentially affected sheet silicates and cordierite, whereas H_2O-free minerals were more stable. All cordierites and five out of six biotites show extremely low $\delta^{18}O$ caused by post-metamorphic effects. Other phases such as feldspars and sillimanite were affected to a lesser degree, whereas quartz and garnet do not show any effects of alteration.

There are good examples of isotopic equilibrium among three minerals formed in stage 1 in mesosomes (LEU 1010.71 I, LEU 1262.96 II, see Table 3). The most reliable thermometer, based on the pair quartz-garnet, yields 621–674 °C, which is consistent with the phase diagram (Fig. 4). The temperature of migmatization (stage 2) could not be deduced from ^{18}O fractionations, because cordierite was hydrothermally altered and the quartz-feldspar fractionation is too small to be used as a thermometer. The temperature of retrograde hydration (stage 3) could be calculated in two samples using albite-muscovite pairs, yielding 417–516 °C. However, significantly lower temperatures result if the Bottinga and Javoy (1973, 1975) calibrations are applied (see Table 3). Temperatures calculated from quartz in leucosomes and retrograde muscovite or albite always indicate disequilibria. Quartz-muscovite temperatures lie above the thermal stability of this assemblage, and ^{18}O enrichment in quartz-albite may even be reversed. This means that migmatitic quartz did not equilibrate with the younger, retrograde fluid.

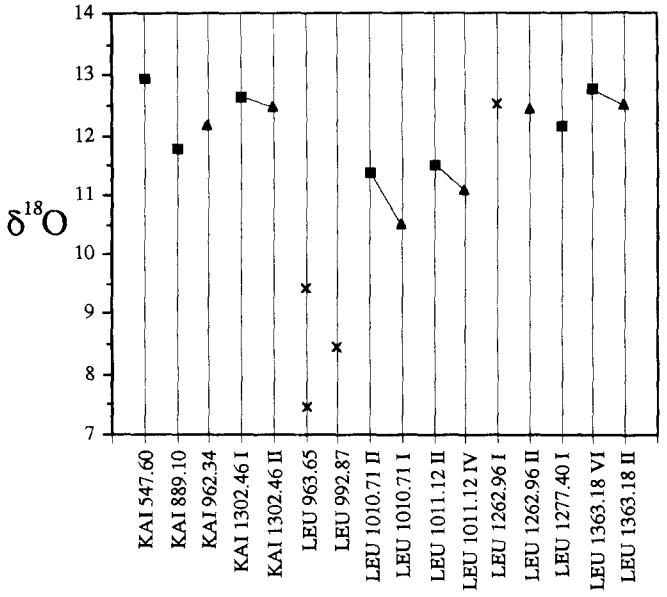

Fig. 6. Measured $\delta^{18}O$ values of quartz. ▲ quartz in mesosomes, melanosomes and homogeneous gneiss, ■ quartz in leucosomes, × quartz in segregations

Origin of H_2O inducing retrograde hydration

Hydrous fluid in equilibrium with retrograde muscovite and albite at 470 °C had a $\delta^{18}O$ of about 10–10.5 ‰, which falls into the field of H_2O coexisting with S-type granites. However, this fluid cannot originate from melt crystallizing in the migmatitic leucosomes, because there was a temperature gap of at least 50 K between the solidus and the upper stability of muscovite + quartz. In this interval any water released by the migmatitic leucosomes must have been expelled from the rocks. During uplift, deeper crustal levels crystallized later, whereas shallower levels had already undergone more advanced cooling. The retrograde hydration observed in the rocks was probably caused by the crystallization of migmatites at greater depth. This crystallization could have taken place at a crustal level about 1.5–2 km deeper than the rocks undergoing retrograde hydration. This hypothesis is consistent with the calculated $\delta^{18}O$ value of the retrograde fluid.

Isotopic effects of hydrothermal alteration

Samples for isotopic analyses were chosen from rock portions that showed minimum hydrothermal alteration (as judged from petrographic criteria). Nonetheless a surprisingly high proportion of the isotopic data unequivo-

cally indicates serious hydrothermal effects that, in many cases, cannot be detected in hand-specimen or in thin section. Hydrothermal effects are characterized by a strong decrease in the $\delta^{18}O$ values of the rocks (down to 5–6‰); $\delta^{18}O$ of biotite can be lowered to almost 0 ‰.

Hydrothermal alteration of the Black Forest basement: previous petrographic and isotopic work

Detailed petrographic studies by Meyer (1985, 1987), Peters (1987), Peters et al. (1989a, b) and ongoing work by the author (e.g. Mazurek 1991) show that the basement of Northern Switzerland was affected by several phases of hydrothermal alteration, each coupled to a brittle deformation event (cataclasis, jointing). The two major types of alteration are:

1. *High temperature alteration*, presumably genetically linked to the intrusion of Variscan granites (mainly during the Upper Carboniferous), characterized by the transformation of plagioclase to albite + sericite and of biotite to chlorite at temperatures around 300–400 °C (as deduced from mineralogy and microthermometric measurements by Mullis and Stalder 1987). Both granites and gneisses were affected.
2. Low-*temperature argillic alteration*, probably linked to tectonic movements and brittle deformation in the Permo-Carboniferous trough of Northern Switzerland (Laubscher 1986, 1987). Plagioclase was altered to clay minerals at temperatures around 100–130 °C as determined from fluid inclusion studies (Mullis and Stalder 1987). Low-temperature alterations are ubiquitous in the Swiss part of the basement; their importance in the Black Forest is not well understood and might be only minor due to the spatial link of this alteration to the North Switzerland Permo-Carboniferous trough.

Hydrothermal alteration is also evident from all recent studies of stable isotopes in Black Forest gneisses and granites (Magaritz and Taylor 1981; Hoefs and Emmermann 1983, Simon and Hoefs 1987; Simon 1989, 1990). In a study covering granites and gneisses from the entire Black Forest, Hoefs and Emmermann (1983) found that the $\delta^{18}O$ distribution of whole-rocks varies widely and extends to very low values (≥ 1.6‰), especially in the Southern Black Forest. They concluded that the low $\delta^{18}O$ rocks have interacted with hydrothermal fluids of meteoric origin and estimated its $\delta^{18}O$ at -9‰. The temperature of alteration was estimated at 300–400 °C and interpreted as a consequence of hydrothermal activity initiated by the intrusion of Variscan granites. There is no doubt that this alteration is identical to the "high-temperature alteration" in the Swiss part of the basement as reported above. Simon (1990) presented $\delta^{18}O$ measurements of minerals from Southern Black Forest granites and confirmed the previous findings that a significant high-temperature hydrothermal alteration had occurred which lowered $\delta^{18}O$ of all minerals except quartz. He also found arguments for a later hydrothermal stage at lower temperatures.

Results

The mean $\delta^{18}O$ values of gneisses and mesosomes lie between 10 and 11‰. However, very low values can also be found (e.g. samples LEU 1010.71, LEU 1011. 12, LEU 1363.18, see Fig. 5), attributable to isotopic exchange of the rock with hydrothermal fluids of meteoric origin. As the mineral data from Table 3 show, hydrothermal alteration generated very large ^{18}O fractionations between slowly exchanging phases such as garnet or quartz and minerals with fast exchange rates such as biotite or cordierite. These findings from the Swiss part of the basement fit well into the scheme of hydrothermal alteration as deduced from isotopic studies from the Black Forest (Hoefs and Emmermann 1983; Simon and Hoefs 1987; Simon 1990).

In Figs. 7 and 8, the mineral data of Table 3 are presented in $\delta^{18}O_{quartz}$–$\delta^{18}O_{mineral}$ diagrams as discussed by Criss et al. (1987), Gregory et al. (1989) and applied to the alteration of Black Forest granites by Simon (1990). Such δ–δ plots can be used to display equilibrium-disequilibrium relations among minerals and they also potentially can provide data on primary (i.e. peak-metamorphic or magmatic) isotopic compositions of hydrothermally altered minerals and ratios of mineral exchange rates if the unaltered protolith can be assumed to be homogeneous.

Discussion

From Fig. 7, which displays rock-forming minerals grown during stages 1 and 2, it is evident that a good part of the

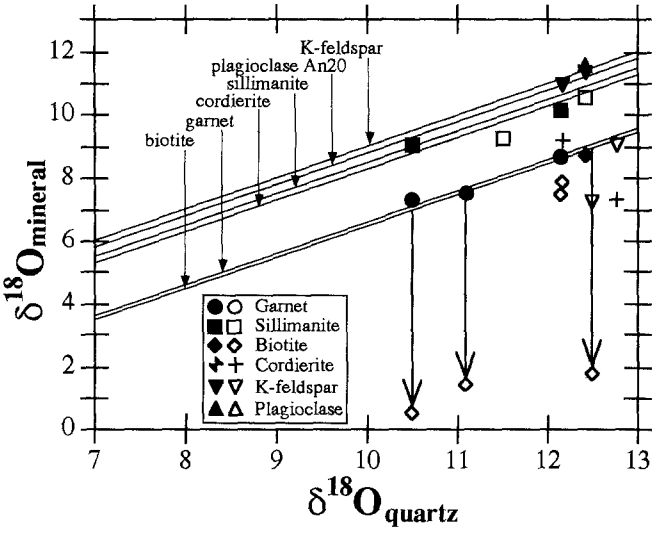

Fig. 7. $\delta^{18}O_{quartz}$-$\delta^{18}O_{mineral}$ diagram for minerals grown at peak-metamorphic conditions (stages 1 and 2), excluding quartz-rich segregations. *Thin lines*, represent equilibrium fractionation isotherms ($\Delta_{quartz-mineral}$) at 640 °C for quartz 1-biotite and -garnet (stage 1 conditions) and at 670–700 °C for quartz 2-feldspars, -sillimanite and -cordierite (stage 2 conditions). Data points falling on the respective isotherm represent equilibrium, *filled symbols*, all other data points, *open symbols*, indicate hydrothermal perturbation of peak-metamorphic equilibria. *Arrows*, indicate hydrothermal effects on biotite. All isotherms calculated using the calibrations of Richter and Hoernes (1988)

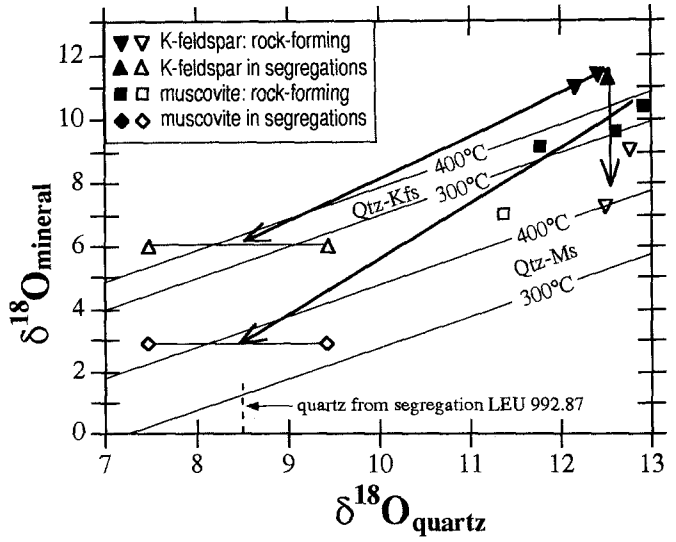

Fig. 8. Diagram of $\delta^{18}O_{quartz}$-$\delta^{18}O_{mineral}$ for minerals occurring in quartz-rich segregations (K-feldspar and muscovite). *Thin lines*, represent equilibrium fractionation isotherms. Segregations are much more strongly affected by hydrothermal alteration than the same mineral pair in the gneisses and migmatites (termed "rock-forming" in the legend). *Filled symbols*, equilibria weakly or not at all affected by hydrothermal effects; *open symbols*, data points affected by hydrothermal exchange. *Arrows*, indicate possible exchange trajectories for quartz-K-feldspar and quartz-muscovite pairs in the segregations

samples has exchanged with hydrothermal fluids under open-system conditions. It can be seen that all quartz-garnet pairs lie very close to the stage 1 isotherm (at 640 °C), indicating the preservation of metamorphic equilibrium. In addition, some quartz-sillimanite, quartz-feldspar and one quartz-biotite pair can be interpreted in terms of preserved peak-metamorphic equilibria because they lie very close to the respective isotherms in Fig. 7. However, many other mineral pairs clearly show hydrothermal effects as indicated by open symbols in Fig. 7. The effect is strongest for biotite which is depleted in ^{18}O down to values of 0.5‰. The data for samples LEU 1010.71 and LEU 1011.12 (Table 3, Fig. 7) are also highly instructive: they show peak-metamorphic equilibrium between quartz and garnet and, in one case, between 3 phases (quartz-garnet-sillimanite). In the same samples, biotite is very strongly depleted in ^{18}O by hydrothermal exchange. Also, sample LEU 1363.18 shows one of the isotopically heaviest values analysed for quartz in spite of a pronounced depletion of biotite. These equilibrium-disequilibrium relations have two implications:

1. Measured $\delta^{18}O$ of rock-forming quartz and garnet (excluding segregations for the moment) reflect peak-metamorphic values. It should be noted that the scatter of these values covers a range of 2‰, due to primary inhomogeneities of the protolith, to migmatitic effects or to other pre-hydrothermal processes. Primary inhomogeneities make the interpretation of hydrothermal exchange trajectories in δ–δ diagrams as developed by Criss et al. (1987) more difficult than in the case of plutonites where the protolith can be assumed to be isotopically homogeneous (e.g. Simon 1990).

2. As quartz and garnet (and in one case also sillimanite) did not exchange to any appreciable amount with hydrothermal fluids even in samples where biotite is strongly depleted, hydrothermal exchange trajectories for quartz-biotite in Fig. 7 are near-vertical as indicated by the arrows. This is consistent with data presented by Hoefs and Emmermann (1983) and Simon (1990) from Black Forest granites and with other examples discussed by Gregory et al. (1989).

Hydrothermal alteration of quartz-rich segregations

The most obvious difference between the segregations and the other rock types discussed above is the fact that even quartz suffered a significant post-metamorphic alteration, which may be caused either by a higher temperature of alteration (> 450 °C, Taylor 1978) or recrystallization due to deformation. Petrographic evidence indicates that the very large (up to 2 cm) quartz crystals present in segregations with low $\delta^{18}O$ have undergone strong plastic deformation, causing subgrain boundary migration and partial dynamic recrystallization. Also, very abundant fluid inclusion trails indicate repeated microcrack formation and healing in these quartz crystals, which gives them a milky appearance in hand specimen. Such features were not identified in quartz from mesosome or leucosome samples. It is suggested that the segregations, due to their low competence, were preferentially deformed during high-temperature alteration and suffered partial recrystallization, as reflected by a hydrothermal isotopic imprint.

Figure 8 shows a δ–δ diagram of quartz-K-feldspar and quartz-muscovite pairs both from segregations and, for comparison, the surrounding migmatitic rocks. One single segregation (which also lacks dynamic recrystallization of quartz in thin section) preserved high $\delta^{18}O$ for K-feldspar and quartz, whereas two other segregations show significant ^{18}O depletions for all minerals (indicated by open symbols; see also Table 3). Depleted quartz has $\delta^{18}O$ values ranging between 7.45 and 9.4‰ within the same segregation; this indicates that no equilibrium was attained between quartz and hydrothermal fluid. Approximate hydrothermal exchange trajectories for quartz-K-feldspar and quartz-muscovite from segregations are also sketched in Fig. 8. In contrast, note that trajectories for quartz-K-feldspar from migmatite samples (i.e. outside the segregations) indicate a near-vertical trend, which means that quartz remained unaltered in those rocks.

Water/rock ratios

Water/rock (W/R) ratios for the altered rocks can be calculated according to Taylor's (1977) open system equation

$$W/R = \ln\left(\frac{\delta_{fluid}^{initial} + \Delta - \delta_{rock}^{initial}}{\delta_{fluid}^{initial} + \Delta - \delta_{rock}^{final}}\right), \quad (23)$$

where Δ is the ^{18}O fractionation between rock and hydrothermal fluid at the temperature of exchange and was calculated using the mineral–water fractionations of

Richter and Hoernes (1988). For the alteration of gneisses/mesosomes, an average mineralogical composition containing 25 vol% quartz and plagioclase (An20), 5% K-feldspar and cordierite, 10% sillimanite, 20% biotite and 10% muscovite was used, yielding values for $\Delta = +2.9‰$ (300 °C) and $+1.2‰$ (400 °C) if quartz is assumed to be inert (as discussed above). The average value of $\delta^{initial}_{rock}$ is taken as 10.5‰ (Fig. 5) and δ^{final}_{rock} as the most-depleted whole-rock identified, i.e. 5.5‰. Assuming $\delta^{initial}_{fluid}$ to be in the range of -12 to $-9‰$ (Hoefs and Emmermann 1983; Simon 1990), W/R ratios are in the range of 0.27–0.36. These values must be considered as minimal because not all fluid interacted completely with the rock and because sampling for the present study was designed to avoid hydrothermal effects wherever possible.

For quartz-rich segregations, an average composition of 80 vol% quartz, 10% K-feldspar and 5% muscovite and albite was used and all phases including quartz (see above) were assumed to exchange isotopes. This gives $\Delta = 7.9‰$ (300 °C) and 4.85‰ (400 °C). The value for $\delta^{initial}_{segregation} = 12.56‰$ is taken from the unaltered segregation LEU 1262.96, and $\delta^{final}_{segregation} = 7.4‰$ corresponds to the most depleted value identified. Assuming interaction of all minerals with the same fluid as in the case of the gneisses, water/rock ratios of 0.30 to 0.47 at 300–400 °C are obtained. This is only slightly higher than the values obtained for the mesosomes. It is concluded that there is no need for significantly higher hydrothermal fluxes in the segregations in order to explain their alteration, but rather a focused deformation that leads to partial recrystallization of quartz.

Summary and conclusions

1. Three distinct phases of metamorphic evolution are documented by petrography, phase relations and oxygen isotope geochemistry.
2. Judging from calculated phase equilibria, migmatite formation took place during regional uplift (pressure decrease).
3. Petrographic evidence indicates that migmatization was anatectic. Leucosomes were not portions of pure melt but rather a mixture of melt, cordierite ± K-feldspar generated by incongruent melting of biotite and sillimanite.
4. Both water-saturated (externally fluxed) and dehydration-melting reactions probably contributed to the generation of melt.
5. The last pervasive isotopic equilibration among all minerals took place during the amphibolite-grade metamorphism of stage 1. This is probably the consequence of recrystallization associated with pervasive deformation of the rocks.
6. The presence of isotopically distinct generations of quartz supports the concept that quartz records the equilibrium isotopic composition during crystal growth and does not exchange subsequently as long as it does not recrystallize (Taylor 1977; Hoernes and Friedrichsen 1978). The fact that in some samples three or four minerals show isotopic equilibrium at temperatures above 600 °C implies that no retrograde isotopic equilibration occurred as suggested by other authors (e.g. Deines 1977; Bowman and Ghent 1986; Huebner et al. 1986; Giletti 1986). This argues for a metamorphic evolution faster than diffusion rates.
7. The rocks were affected by several phases of hydrothermal alteration. The most prominent phase is linked to the intrusion of Variscan granites and caused significant decrease of $\delta^{18}O$ of the rocks.
8. Sheet silicates, cordierite and feldspars are most strongly affected by hydrothermal exchange of oxygen isotopes, which is not necessarily detectable from petrographic evidence.
9. Quartz remained unaffected by hydrothermal effects except in quartz-rich segregations where it was very strongly deformed and even partially recrystallized.
10. The approach of Richter and Hoernes (1988) for the calculation of isotopic temperatures yields reasonable results. Temperatures calculated for stages 1 and 3 are consistent with phase petrology.

Acknowledgements. I thank my advisors, Martin Frey and Rudolf Hänny, for their support during the project. Discussions with Jürg Meyer, Jürgen Abrecht and Tjerk Peters helped to clarify many problems. Careful reviews by Jürgen Abrecht, Josh Lieberman, Peter Mozley, David Pattison and two unknown reviewers improved the manuscript. The core material for this study was kindly supplied by NAGRA (Swiss national cooperative for the storage of radioactive waste). Special thanks go to S. Hoernes who not only produced the stable isotope data but also contributed in several discussions. This paper is part of the author's Ph.D. thesis. Financial support by the Swiss National Science Foundation (grant no. 2.578–0.84 to M. Frey) is gratefully acknowledged.

References

Abrecht J (1980) Zur Bildung migmatitischer Schollenamphibolite aus dem Altkristallin des Aarmassivs. Geol Rundsch 69:695–725
Ashworth JR (1976) Petrogenesis of migmatites in the Huntly-Portsoy area, North-East Scotland. Mineral Mag 40:661–682
Ashworth JR (1985) Migmatites. Blackie, Glasgow
Berman RG (1988) Internally-consistent thermodynamic data for stoichiometric minerals in the system Na_2O–K_2O–CaO–MgO–FeO–Fe_2O_3–Al_2O_3–SiO_2–TiO_2–H_2O–CO_2. J Petrol 29:445–522
Berman RG (1990) Mixing properties of Ca–Mg–Fe–Mn garnets. Am Mineral 75:328–344
Bottinga Y, Javoy M (1973) Comments on oxygen isotope geothermometry. Earth Planet Sci Lett 20:250–265
Bottinga Y, Javoy M (1975) Oxygen isotope partitioning among the minerals in igneous and metamorphic rocks. Rev Geophys Space Phys 13:401–418
Bowman JR, Ghent ED (1986) Oxygen and hydrogen isotope study of minerals from metapelitic rocks, staurolite to sillimanite zones, Mica Creek, British Columbia. J Metamorphic Geol 4:131–141
Brown TH, Berman RG, Perkins EH (1989) PTA-SYSTEM: a GeO-Calc software package for the calculation and display of activity-temperature-pressure phase diagrams. Am Mineral 74:485–487
Büsch W (1966) Petrographie und Abfolge der Granitisation im Schwarzwald V. Neues Jahrb Mineral Abh 104:190–258
Chatterjee ND, Froese E (1975) A thermodynamic study of the pseudobinary join muscovite-paragonite in the system $KAlSi_3O_8$–$NaAlSi_3O_8$–Al_2O_3–SiO_2–H_2O. Am Mineral 60:985–993
Chiba H, Chacko T, Clayton RN, Goldsmith JR (1989) Oxygen isotope fractionations involving diopside, forsterite, magnetite, and calcite: application to geothermometry. Geochim Cosmochim Acta 53:2985–2995

Clayton RN, Goldsmith JR, Mayeda TK (1989) Oxygen isotope fractionation in quartz, albite, anorthite and calcite. Geochim Cosmochim Acta 53:725–733

Criss RE, Gregory RT, Taylor HP (1987) Kinetic theory of oxygen isotopic exchange between minerals and water. Geochim Cosmochim Acta 51:1099–1108

Deines P (1977) On the oxygen isotope distribution among mineral triplets in igneous and metamorphic rocks. Geochim Cosmochim Acta 41:1709–1730

De La Roche H (1972) Revue sommaire de quelques diagrammes chimico-minéralogiques pour l'étude des associations ignées ou sédimentaires et de leurs dérioés métamorphiques. Sci Terre 17:1–2

Fuhrman ML, Lindsley DH (1988) Ternary-feldspar modeling and thermometry. Am Mineral 73:201–216

Garlick GD (1966) Oxygen isotope fractionation in igneous rocks. Earth Planet Sci Lett 1:361–368

Garrels RM, MacKenzie FT (1971) Evolution of sedimentary rocks. Morton, New York

Giletti BJ (1986) Diffusion effects on oxygen isotope temperatures of slowly cooled igneous and metamorphic rocks. Earth Planet Sci Lett 77:218–228

Graham CM, Greig KM, Sheppard SMF, Turi B (1983) Genesis and mobility of the H_2O–CO_2 fluid phase during regional greenschist and epidote amphibolite facies metamorphism: a petrological and stable isotope study in the Scottish Dalradian. J Geol Soc London 140:577–600

Grant JA (1985) Phase equilibria in partial melting of pelitic rocks. In: Ashworth JR (ed) Migmatites. Blackie, Glasgow, pp 86–144

Gregory RT, Criss RE, Taylor HP (1989) Oxygen isotope exchange kinetics of mineral pairs in closed and open systems: applications to problems of hydrothermal alteration of igneous rocks and Precambrian iron formations. Chem Geol 75:1–42

Haar L, Gallagher J, Kell GS (1984) NBS/NRC Steam Tables: thermodynamic and transport properties and computer programs for vapor and liquid states of water in SI units. Hemisphere, Washington

Henkes L, Johannes W (1981) The petrology of a migmatite (Arvika, Värmland, western Sweden). Neues Jahrb Mineral Abh 141:113–133

Hoefs J (1987) Stable isotope geochemistry, 3rd edn. Springer, Berlin Heidelberg New York

Hoefs J, Emmermann R (1983) The oxygen isotope composition of Hercynian granites and Pre-Hercynian gneisses from the Schwarzwald, Germany. Contrib Mineral Petrol 83:320–329

Hoernes S, Friedrichsen H (1978) Oxygen and hydrogen isotope study of the polymetamorphic area of the Northern Oetztal-Stubai Alps (Tyrol). Contrib Mineral Petrol 67:305–315

Hoffer E (1978) Melting reactions in aluminous metapelites: stability limits of biotite + sillimanite + quartz in the presence of albite. Neues Jahrb Mineral Monatsh 1978:396–407

Hofmann A, Köhler H (1973) Whole-rock Rb-Sr ages of anatectic gneisses from the Schwarzwald, SW Germany. Neues Jahrb Mineral Abh 119:163–187

Huebner M, Kyser TK, Nisbet EG (1986) Stable-isotope geochemistry of high-grade metapelites from the Central Zone of the Limpopo belt. Am Mineral 71:1343–1353

Indares A, Martignole J (1985) Biotite-garnet geothermometry in the granulite facies: the influence of Ti and Al in biotite. Am Mineral 70:272–278

Johannes W (1978) Melting of plagioclase in the system Ab–An–H_2O and Qz–Ab–An–H_2O at P_{H2O} = 5 kbars, an equilibrium problem. Contrib Mineral Petrol 66:295–303

Johannes W (1983) Metastable melting in granite and related systems. In: Atherton MP, Gribble CD (eds) Migmatites, melting and metamorphism. Shiva, Nantwich, pp 27–36

Johannes W (1985) The significance of experimental studies for the formation of migmatites. In: Ashworth JR (ed) Migmatites. Blackie, Glasgow, pp 36–85

Kieffer SW (1982) Thermodynamics and lattice vibrations of minerals. 5: applications to phase equilibria, isotopic fractionation, and high-pressure thermodynamic properties. Rev Geophys Space Phys 20:827–849

Klein H, Wimmenauer W (1984) Eclogites and their retrograde transformation in the Schwarzwald (Fed. Rep. Germany). Neues Jahrb Mineral Monatsh 1984:25–38

Kretz R (1983) Symbols for rock-forming minerals. Am Mineral 68:277–279

Laubscher HP (1986) The Eastern Jura: relations between thin-skinned and basement tectonics, local and regional. Geol Rundsch 75:535–553

Laubscher HP (1987) Die tektonische Entwicklung der Nordschweiz. Eclogae Geol Helv 80: 287–303

Le Breton N, Thompson AB (1988) Fluid-absent (dehydration) melting of biotite in metapelites in the early stages of crustal anatexis. Contrib Mineral Petrol 99:226–237

Loomis TP (1983) Compositional zoning of crystals: a record of growth and reaction history. In: Saxena SK (ed) Kinetics and equilibrium in mineral reactions. (Advances in Physical geochemistry, vol 3) Springer, Berlin Heidelberg New York, pp. 1–60

Magaritz M, Taylor HP (1981) Low $\delta^{18}O$ migmatites and schists from the tectonic contact zone between Hercynian (= Variscan) granites and the older gneissic core complex of the Black Forest (Schwarzwald), West Germany (abstract). Abstr Annu Meeting Geol Soc Am 13:501

Mazurek M (1988) Petrogenese metapelitischer Migmatite aus Bohrungen der Nordwestschweiz. Unpubl PhD thesis, Univ Basel

Mazurek M (1991) Water flowpaths in fractured crystalline rock (abstract). Terra Abstr 3:187

McPhail DC (1985) The stability of Mg-chlorite. Unpubl MSc thesis, Univ British Columbia, Vancouver

Mehnert KR (1953, 1957, 1962, 1963) Petrographie und Abfolge der Granitisation im Schwarzwald I-IV. Neues Jahrb Mineral Abh 85:59–140; 90:39–90; 98:208–249; 99:161–199

Mehnert KR (1968) Migmatites and the origin of granitic rocks. Elsevier, Amsterdam

Metz R (1980) Geologische Landeskunde des Hotzenwaldes. Moritz Schauenburg, Lahr/Schwarzwald

Meyer J (1985) Hydrothermale Umwandlungen und postmetamorphe Deformationen im Kristallin der NAGRA-Bohrung Kaisten. Schweiz Mineral Petrogr Mitt 65:363–364

Meyer J (1987) Die Kataklase im kristallinen Untergrund der Nordschweiz. Eclogae Geol Helv 80:323–334

Mullis J, Stalder HA (1987) Salt-poor and salt-rich fluid inclusions in quartz from two boreholes in Northern Switzerland. Chem Geol 61:263–272

O'Neil JR, Chappell BW (1977) Oxygen and hydrogen isotope relations in the Berridale batholith. J Geol Soc London 133:559–571

Patel A, Mendelssohn MJ, Price GD (1989) Oxygen isotope partitioning between silicates: computer simulation approach (abstract). Terra Abstr 1:346

Patiño Douce AE, Johnston AD (1991) Phase equilibria and melt productivity in the pelitic system: implications for the origin of peraluminous granitoids and aluminous granulites. Contrib Mineral Petrol 107:202–218

Pattison DRM (1989) *P–T* conditions and the influence of graphite on pelitic phase relations in the Ballachulish aureole, Scotland. J Petrol 30:1219–1244

Perkins EH, Brown TH, Berman RG (1986) PT-SYSTEM, TX-SYSTEM, PX-SYSTEM: three programs which calculate pressure-temperature-composition phase diagrams. Comput Geosci 12:749–755

Peters T (1987) Das Kristallin der Nordschweiz: Petrographie und hydrothermale Umwandlungen. Eclogae Geol Helv 80:305–322

Peters T, Matter A, Bläsi HR, Isenschmid C, Kleboth P, Meyer C, Meyer J (eds) (1989a) Sondierbohrung Leuggern-Geologie. Nagra (CH-Baden) Technischer Bericht NTB 86–05

Peters T, Matter A, Meyer J, Isenschmid C, Ziegler HJ (eds) (1989b) Sondierbohrung Kaisten-Geologie. Nagra (CH-Baden) Technischer Bericht NTB 86–04

Powell R, Holland T (1990) Calculated mineral equilibria in the

pelite system, KFMASH (K_2O–FeO–MgO–Al_2O_3–SiO_2–H_2O). Am Mineral 75:367–380
Puziewicz J, Johannes W (1988) Phase equilibria and compositions of Fe–Mg–Al minerals and melts in water-saturated peraluminous granitic systems. Contrib Mineral Petrol 100:156–168
Richter R, Hoernes S (1988) The application of the increment method in comparison with experimentally derived and calculated O-isotope fractionations. Chem Erde 48:1–18
Rutishauser H, Hügi T (1978) Der Kontakt zwischen Gasterngranit und Lauterbrunner Kristallin im Gasterntal (Aarmassiv, Schweiz). Mitt Naturforsch Ges Bern nF 35:3–53
Schaltegger U (1986) Voralpine und alpine Mineralbildung in der Gneiszone von Erstfeld in der Umgebung von Erstfeld (Sustenpass, Aarmassiv); der Mechanismus der K-Ar und Rb-Sr-Verjüngung alpin umgewandelter Biotite. Schweiz Mineral Petrogr Mitt 66:395–412
Schütze H (1980) Der Isotopenindex-Eine Inkrementenmethode zur näherungsweisen Berechnung von Isotopenaustauschgleichgewichten zwischen kristallinen Substanzen. Chem Erde 39:321–334
Sheppard SMF (1977) The Cornubian batholith, SW England: D/H and $^{18}O/^{16}O$ studies of kaolinite and other alteration minerals. J Geol Soc London 133:573–591
Sheppard SMF (1986) Characterization and isotopic variations in natural waters. In: Valley JW, Taylor HP, O'Neil JR (eds) Stable isotopes in high temperature geological processes (Reviews in Mineralogy 16). Mineral Soc Am Washington, D.C., pp 165–184
Sheppard SMF, Nielsen RL, Taylor HP (1969) Oxygen and hydrogen isotope ratios of clay minerals from porphyry copper deposits. Econ Geol 64:755–777
Simon K (1989) Water/rock interaction in Southern Schwarzwald granites: O, H-isotope and trace element study (abstract). Terra Abstr 1:329
Simon K (1990) Hydrothermal alteration of Variscan granites, southern Schwarzwald, Federal Republic of Germany. Contrib Mineral Petrol 105:177–196
Simon K, Hoefs J (1987) Effects of meteoric water interaction on Hercynian granites from the Südschwarzwald, Southwest Germany. Chem Geol 61:253–261
Spear FS, Cheney JT (1990) A petrogenetic grid for pelitic schists in the system SiO_2–Al_2O_3–FeO–MgO–K_2O–H_2O. Contrib Mineral Petrol 101:149–164
Steiger RH, Bär MT, Büsch W (1973) The zircon age of an anatectic rock in the central Schwarzwald. Fortschr Mineral 50:131–132
Taylor HP (1977) Water/rock interactions and the origin of H_2O in granitic batholiths. J Geol Soc London 133:509–558.
Taylor HP (1978) Oxygen and hydrogen isotope studies of plutonic granitic rocks. Earth Planet Sci Lett 38:177–210
Taylor HP, Epstein S (1962) Relation between $^{18}O/^{16}O$ ratios in coexisting minerals of igneous and metamorphic rocks. I:principles and experimental results. Bull Geol Soc Am 73:461–480
Taylor HP, Sheppard SMF (1986) Igneous rocks. I: processes of isotopic fractionation and isotope systematics. In: Valley JW, Taylor HP, O'Neil JR (eds) Stable isotopes in high temperature geological processes (Reviews in Mineralogy 16). Mineral Soc Am, Washington, D.C., pp 227–272
Thompson AB (1982) Dehydration melting of pelitic rocks and the generation of H_2O-undersaturated liquids. Am J Sci 282:1567–1595
Vielzeuf D, Boivin P (1984) An algorithm for the construction of petrogenetic grids: application to some equilibria in granulitic paragneisses. Am J Sci 284:760–791
Vielzeuf D, Holloway JR (1988) Experimental determination of the fluid-absent melting reactions in the pelitic system. Contrib Mineral Petrol 98:257–276
Von Raumer JF (1983) Die Metapelite von Emosson (Aiguilles Rouges-Massiv) als Beispiel späkaledonisch-frühvariszischer Metamorphose im Altkristallin des helvetischen Bereichs. Schweiz Mineral Petrogr Mitt 63:421–455
Wimmenauer W (1984) Das prävariskische Kristallin im Schwarzwald. Fortschr Mineral Beih 2, 62:69–86
Wimmenauer W (1985) The pre-Variscan basement of the Schwarzwald– a target area of a deep research drilling. 2nd international symposium on observation of the continental crust through drilling–excursion guide Schwarzwald, pp 1–7
Yoder HS, Stewart DB, Smith JR (1957) Ternary feldspars. Carnegie Inst Washington Yearb 56:206–214

Editorial responsibility: J. Hoefs